Title

Extracellular vesicles transfer nuclear Abl-dependent and radiation-induced miR-34c into unirradiated cells to cause bystander effects.

Journal

Molecular biology of the cell, 29(18)

ISSN

1059-1524

Authors

Rastogi, Shubhra
Hwang, Amini
Chan, Josolyn
et al.

Publication Date

2018-09-01

DOI

10.1091/mbc.e18-02-0130

Peer reviewed

Extracellular vesicles transfer nuclear Abl-dependent and radiation-induced miR-34c into unirradiated cells to cause bystander effects

Shubhra Rastogi, Amini Hwang, Josolyn Chan, and Jean Y. J. Wang*
Division of Hematology–Oncology, Department of Medicine, School of Medicine, University of California, San Diego, La Jolla, CA 92093-0644

ABSTRACT **Ionizing radiation (IR) not only activates DNA damage response (DDR) in irradiated cells but also induces bystander effects (BE) in cells not directly targeted by radiation. How DDR pathways activated in irradiated cells stimulate BE is not well understood. We show here that extracellular vesicles secreted by irradiated cells (EV-IR), but not those from unirradiated controls (EV-C), inhibit colony formation in unirradiated cells by inducing reactive oxygen species (ROS). We found that μEV-IR from Abl nuclear localization signal–mutated (*Abl-μNLS*) cells could not induce ROS, but expression of wild-type Abl restored that activity. Because nuclear Abl stimulates miR-34c biogenesis, we measured miR-34c in EV and found that its levels correlated with the ROS-inducing activity of EV. We then showed that EV from miR-34c minigene–transfected, but unirradiated cells induced ROS; and transfection with miR-34c-mimic, without radiation or EV addition, also induced ROS. Furthermore, EV-IR from miR34-family triple-knockout cells could not induce ROS, whereas EV-IR from wild-type cells could cause miR-34c increase and ROS induction in the miR-34 triple-knockout cells. These results establish a novel role for extracellular vesicles in transferring nuclear Abl-dependent and radiation-induced miR-34c into unirradiated cells to cause bystander oxidative stress.**

Monitoring Editor
Kunxin Luo
University of California, Berkeley

Received: Feb 20, 2018
Revised: Jun 1, 2018
Accepted: Jun 27, 2018

INTRODUCTION

Ionizing radiation (IR) causes oxidative stress and DNA damage that activate a wide range of biological responses in cells that are directly targeted by the radiation energy. In multicellular organisms, radiation also induces bystander effects (RIBE) in neighboring or distant cells not targeted by IR (Prise and O'Sullivan, 2009; Mukherjee *et al.*, 2014; Verma and Tiku, 2017). The nontarget, or bystander, effects of IR occur when irradiated cells secrete soluble factors and/or extracellular vesicles (EV) to propagate the damage signal to naïve, unirradiated responder cells (Prise and O'Sullivan, 2009; Mukherjee *et al.*, 2014; Jelonek *et al.*, 2016; Verma and Tiku, 2017). The master regulators of DNA damage response (DDR), ATM and p53, are required for irradiated cells to secrete bystander effectors (Komarova *et al.*, 1998; Burdak-Rothkamm *et al.*, 2008); however, how other DDR pathways participate in the transmission of RIBE signals is mostly unknown.

Previous studies have established that IR stimulates nuclear Abl tyrosine kinase to regulate transcription, DNA repair, and microRNA (miR) processing (Baskaran *et al.*, 1997; Shaul and Ben-Yehoyada, 2005; Preyer *et al.*, 2007; Kaidi and Jackson, 2013; Wang, 2014; Tu *et al.*, 2015). The ubiquitously expressed Abl has many context-dependent biological functions that are determined by its activating signals, its interacting proteins, and its subcellular localization (Wang, 2014). We have been investigating the biological functions of Abl in DDR, and because the DNA damage signal initiates in the nucleus, we have focused on the nuclear Abl. To identify the essential functions of nuclear Abl in DDR, we mutated the three nuclear-localization signals (NLS) in the mouse *Abl1* gene to create the *Abl-μNLS* (*μ*) allele (Preyer *et al.*, 2007). While the $Abl^{-/-}$ mice show

This article was published online ahead of print in MBoC in Press (http://www.molbiolcell.org/cgi/doi/10.1091/mbc.E18-02-0130) on July 5, 2018.

Author contributions: S.R. designed and performed the experiments, analyzed the data, and wrote the paper. A.H. and J.C. performed experiments and analyzed the data. J.Y.J.W. conceived of the idea, designed the experiments, analyzed the data, and wrote the paper.

*Address correspondence to: Jean Y.J. Wang (jywang@ucsd.edu).

Abbreviations used: DDR, DNA damage response; EV, extracellular vesicles; IR, ionizing radiation; NLS, nuclear localization signal; ROS, reactive oxygen species.

a wide range of developmental defects and suffer from embryonic and neonatal lethality, the $Abl^{\mu/\mu}$ mice are healthy and fertile (Sridevi *et al.*, 2013). However, DNA damage–induced apoptosis is defective in the $Abl^{\mu/\mu}$ embryonic stem cells and in the renal proximal tubule epithelial cells (RPTC) of the $Abl^{\mu/\mu}$ mice (Preyer *et al.*, 2007; Sridevi *et al.*, 2013). Thus, studies of the *Abl-μNLS* mutant mice have provided in vivo evidence for the conclusion that DNA damage activates nuclear Abl to stimulate apoptosis (Gong *et al.*, 1999). To identify nuclear Abl-stimulated proapoptotic factors, we searched for DNA damage–induced microRNA that required nuclear Abl for expression, because several microRNAs have been implicated as apoptosis promoters in DDR (He *et al.*, 2007). In a previous study, we found that Abl kinase phosphorylates the DGCR8 subunit of the microprocessor complex to stimulate the processing of miR-34c (Tu *et al.*, 2015). We also showed that DNA damage-induced expression of miR-34c is defective in the *Abl-μNLS* mice (Tu *et al.*, 2015).

Transcription of the miR-34-family of microRNAs is activated by p53 in DDR (He *et al.*, 2007). In cell-based studies, miR-34a is found to promote apoptosis (Chang *et al.*, 2007; Raver-Shapira *et al.*, 2007). However, mouse genetics study has shown that p53-dependent apoptosis is not diminished in mice with single knockout of miR-34a or triple knockout (TKO) of the three members (a, b, c) of the miR-34 family (Concepcion *et al.*, 2012). The finding that the miR-34 family of microRNAs are not essential to DNA damage–induced apoptosis in mice inspired us to consider alternative functions for the Abl-miR34c pathway in DDR. It has been shown that extracellular vesicles (EV) can transfer microRNA between cells (Tkach and Thery, 2016; Valadi *et al.*, 2007). Recent results have also suggested that EV and microRNA are involved in the communication between irradiated and bystander cells (Chaudhry, 2014; Jelonek *et al.*, 2016). Therefore, we investigated the role of nuclear Abl, miR-34c, and EV in RIBE and found that EV could indeed transfer miR-34c from irradiated cells to unirradiated cells to cause oxidative stress.

RESULTS

Isolation and characterization of extracellular vesicles

We isolated EV by differential ultracentrifugation from media conditioned by unirradiated (Con) or irradiated (IR) mouse embryo fibroblasts (MEFs) (Figure 1A). Nanoparticle tracking analyses showed comparable size distributions and particle concentrations between EV-C isolated from media of unirradiated MEFs and EV-IR isolated from media of irradiated MEFs (Figure 1B). As the particles ranged from 50 to 300 nm in diameter, these EV preparations were likely to contain a mixture of microvesicles derived from different intracellular compartments (Cocucci *et al.*, 2009). The total protein (Figure 1C) and RNA content (Figure 1D) of multiple independent EV-C and EV-IR preparations was comparable, showing that IR did not significantly affect the overall production of EV. When added to naïve, unirradiated responder MEFs, fluorescently labeled EV-C and EV-IR were internalized by 98–100% of cells at 24 h (Figure 1E) and to comparable intracellular levels (Figure 1F). Thus, the differential response of unirradiated MEFs to EV-C and EV-IR was unlikely to be due to differential uptake of these vesicles.

To compare EV preparations from different producer cells used in this study, we calculated the protein-to-particle ratios of EV preparations from MEFs with different *Abl* genotypes and found that neither irradiation nor *Abl* genotypes had a significant effect on those ratios (Figure 1G). The protein-to-particle ratios of EV from HEK293T cells were also comparable and not affected by the transfected plasmid DNA (Figure 1G). The protein-to-particle ratios of EV produced by MEFs, however, were significantly different from those produced by HEK293T cells (Figure 1G). These results showed that the biological activity of EV from MEFs of different *Abl*-genotypes could be compared by normalizing for EV protein.

EV-IR but not EV-C inhibited colony formation

Inhibition of colony formation is both a direct and a bystander effect of ionizing radiation (Mladenov *et al.*, 2018), as media conditioned by irradiated MEFs (CM-IR) inhibited colony formation when transferred to unirradiated responder MEFs (Figure 2, A and B). We found that the EV fraction retained the colony-inhibitory activity of CM-IR, whereas the supernatant fraction lost most of that activity (Figure 2, A and B). Titration experiments showed that EV-IR inhibited colony formation in a dose-dependent manner, reaching saturation at an EV-protein level (100 μg) that was equivalent to around 20 million particles per responder cell (Figure 2, E and F). In contrast, EV-C did not elicit such a dose response (Figure 2, C and D). Previous studies have suggested that irradiated cells secrete inducers of reactive oxygen species (ROS) to inhibit colony formation in bystander cells (Mladenov *et al.*, 2018). Consistent with those results, we found that treatment of responder MEFs with the anti-oxidant N-acetylcysteine (NAC) interfered with the colony-inhibitory activity of EV-IR (Figure 2, G and H). Taken together, these results showed that irradiated MEFs secreted extracellular vesicles with colony-inhibitory activity.

EV-IR but not EV-C increased reactive oxygen species

To measure the effect of EV-C and EV-IR on the levels of reactive oxygen species (ROS), we labeled live responder cells with fluorescent dyes at 24 h after EV addition and determined the ROS/cell volume ratio by digital imaging (Figure 3). We found that EV-IR, but not EV-C, increased the ROS levels in unirradiated MEFs (Figure 3, A–C). The ROS increase also showed EV-IR dose dependency: induction of ROS was detectable at 3.75 μg of EV-IR and reached a peak at 25 μg of EV-IR (Figure 3D). Treatment of responder cells with the anti-oxidant NAC neutralized EV-IR–induced ROS increase (Figure 3, B and C, EV-IR+NAC). Because NAC also interfered with the colony-inhibitory activity of EV-IR (Figure 2, G and H), these results suggested that ROS was a major factor contributing to EV-IR-induced inhibition of colony formation. Treatment with proteinase K or RNase A did not abolish either the colony-inhibitory or the ROS-inducing activity of EV-IR (Figure 3E), indicating that this activity was mediated by factors inside the vesicles.

IR-induced reactive oxygen species in *Abl-μNLS* mouse embryo fibroblasts but μEV-IR could not induce reactive oxygen species in unirradiated cells

To determine the essential function of nuclear Abl in DDR, we constructed the *Abl-μNLS* allele in the mouse *Abl1* gene by mutating the three nuclear-localization signals (NLS) in the Abl protein (Figure 4A; Preyer *et al.*, 2007). We established embryo fibroblasts (MEFs) from littermate $Abl^{+/+}$ (*Abl-wt*) and $Abl^{\mu/\mu}$ (*Abl-μNLS*) mice through serial passages in culture (Sridevi *et al.*, 2013). Irradiation of *Abl-wt* MEFs significantly increased the nuclear levels of Abl protein, whereas irradiation of *Abl-μNLS* MEFs had no such effect (Figure 4, B and C). Thus, mutation of the NLS is sufficient to abolish IR-induced Abl nuclear accumulation. Despite this defect, we found that IR still induced ROS in the *Abl-μNLS* MEFs (Figure 4, D and E).

We then isolated μEV-C and μEV-IR from control and irradiated *Abl-μNLS* MEFs, respectively. The μEV preparations consistently showed similar levels of total protein and RNA when compared with EV preparations from *Abl-wt* MEFs (Figure 4, F and G). The

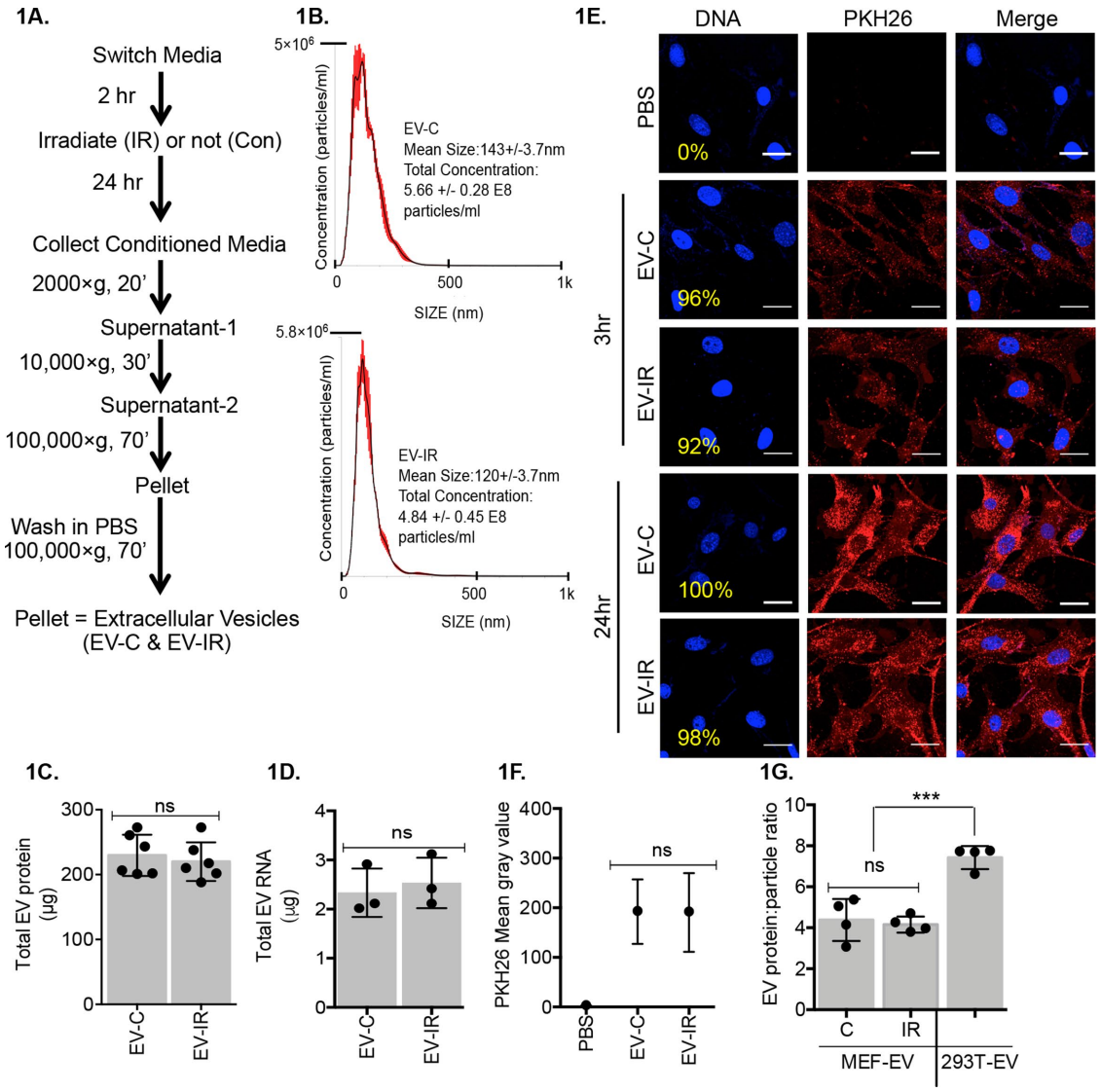

FIGURE 1: Isolation, quantification, and uptake of extracellular vesicles. (A) Flowchart summarizing the EV isolation protocol: EV-C from media of unirradiated (Con) cells and EV-IR from media of irradiated (IR) cells. (B) Nanoparticle tracking analysis of EV-C and EV-IR. (C) Total protein in EV-C and EV-IR from 100 ml of conditioned media. Values shown are mean ± SD of six independent EV preparations. ns, not significant, one-way ANOVA. (D) Total RNA in EV-C and EV-IR from 100 ml of conditioned media. Values shown are mean ± SD of three independent EV preparations. ns, not significant, one-way ANOVA. (E) Uptake of PKH26-labeled EV-C (25 μg) and EV-IR (25 μg) by unirradiated MEFs detected by fluorescence microscopy at 3 and 24 h after EV addition. Representative images (scale bar 35 μm) with the percentage of cells stained positive for PKH26 indicated. Note that PKH26 dye was added to the PBS sample, but the signal was too dilute to be visualized. (F) Quantification of PKH26 mean gray values in MEFs treated with PKH26-PBS, PKH26-EV-C (25 μg), or PKH26-EV-IR (25 μg). The mean ± SD from at least six images are shown. ns, not significant, one-way ANOVA. (G) Protein-to-particle ratios of EV preparations from MEFs and HEK293T cells. MEF-EV (C): protein-to-particle ratios from EV-C, μEV-C, μEV-C-Abl^{WT}, μEV-C-Abl$^{\mu NLS}$. MEF-EV (IR): ratios from EV-IR, μEV-IR, μEV-IR-Abl^{WT}, μEV-IR-Abl$^{\mu NLS}$. 293T-EV: ratios from EV-Vector, EV-AblPPn, EV-miR34c, EV-miR34c+AblPPn. Values shown are mean ± SD. ns, not significant, ***$P < 0.001$, one-way ANOVA.

protein-to-particle ratios of μEV were also similar to those of EV (Figure 1G). Thus, the *μNLS* mutation did not affect the overall production of EV. However, we found that μEV-IR could not induce ROS when added to unirradiated cells (Figure 4, H and I), despite the ROS increase in the irradiated *Abl-μNLS* producers (Figure 4, D and E). Together, these results showed that nuclear Abl is not required for IR to induce ROS, but its absence prevented irradiated cells from producing EV-IR with ROS-inducing activity.

Expression of Abl^{WT} in *Abl-μNLS* mouse embryo fibroblasts restored reactive oxygen species–inducing activity to μEV-IR

To determine whether restoration of nuclear Abl could rescue the ROS-inducing activity of μEV-IR, we stably expressed Abl^{WT} or Abl$^{\mu NLS}$ in *Abl-μNLS* MEFs through retrovirus-mediated gene transfer (Figure 5A) without significantly raising the steady state levels of Abl protein (Figure 5B). After irradiation, nuclear Abl increased in the *Abl-μNLS*-Abl^{WT} but not the *Abl-μNLS*-Abl$^{\mu NLS}$ MEFs (Figure 5, C and D).

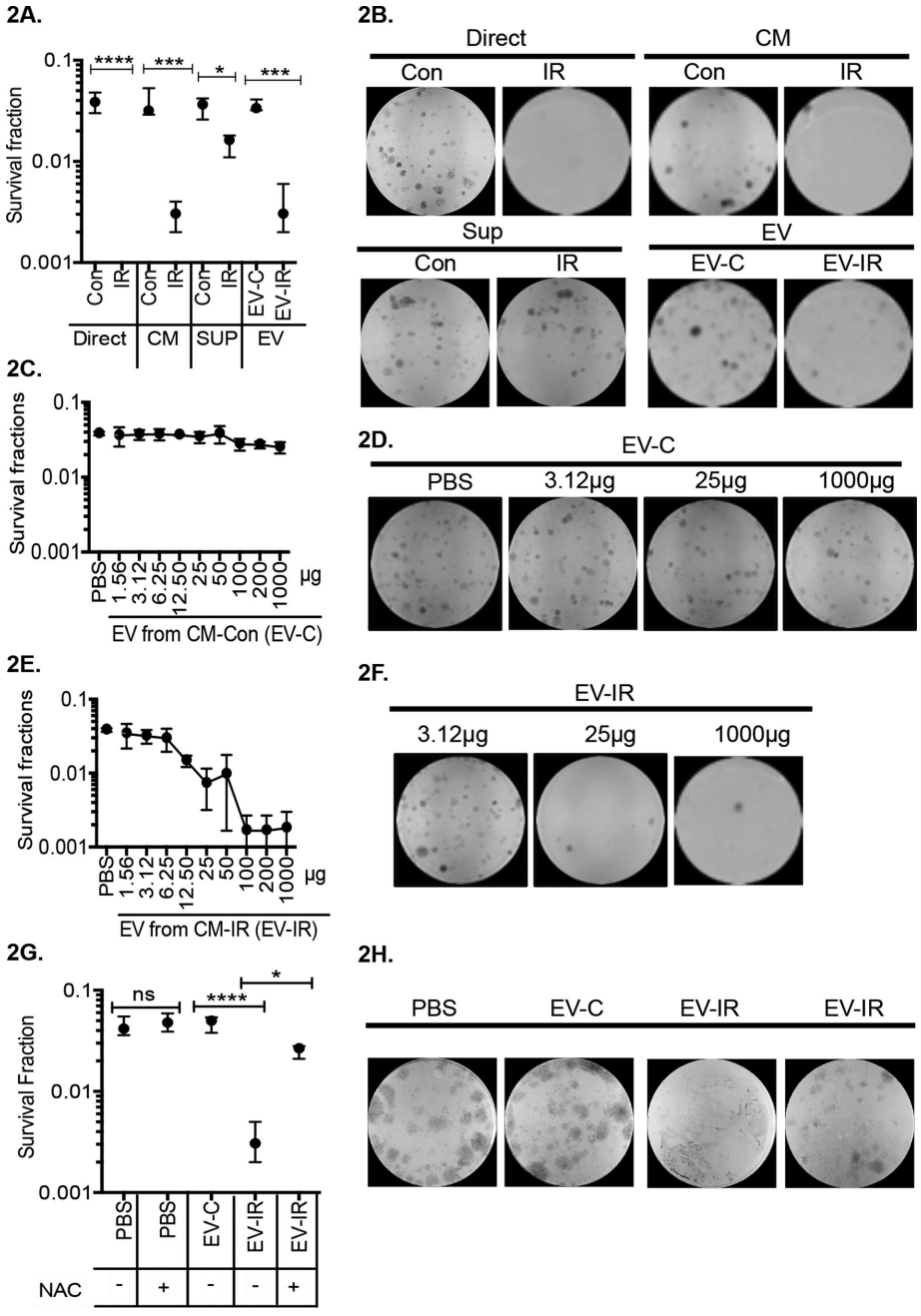

FIGURE 2: Extracellular vesicles from irradiated cells (EV-IR) inhibited colony formation. (A) Clonogenic survival fractions and (B) representative images of MEFs at 15 d after the following treatments: unirradiated (Direct, Con), irradiated (Direct, IR, 10Gy), treated for 24 h with CM (conditioned media), Sup (supernatant-2 of CM), EV-C or EV-IR (25µg each) from unirradiated (Con) or irradiated (IR) MEFs (see Figure 1A). Values shown are mean ± SD from three independent experiments. *$P < 0.05$, ***$P < 0.001$, ****$P < 0.0001$, one-way ANOVA. (C) Clonogenic survival fractions and (D) representative images of MEFs at 15 d after treatment with PBS or the indicated amounts of EV-C for 24 h. Values shown are mean ± SD from two independent experiments. (E) Clonogenic survival fractions and (F) representative images of MEFs at 15 d after treatment with PBS or the indicated amounts of EV-IR for 24 h. Values shown are mean ± SD from two independent experiments. (G) Clonogenic survival fractions and (H) representative images of MEFs at 15 d after the indicated treatments for 24 h. NAC: N-acetylcysteine (5 mM). EV-C and EV-IR: 25 µg each. Values shown are mean ± SD from three independent experiments. ns, not significant, *$P < 0.05$, ****$P < 0.0001$, one-way ANOVA.

Because the exogenous Abl^{WT} was not overproduced relative to the endogenous $Abl^{\mu NLS}$ (Figure 5B), the IR-induced increase in nuclear Abl was less in *Abl-µNLS*-Abl^{WT} cells than in *Abl-wt* cells (compare Figure 5D with Figure 4C). The expression of Abl^{WT} or $Abl^{\mu NLS}$ did not alter the direct effect of IR on ROS (Figure 5, E and F), again showing that nuclear Abl did not contribute to ROS induction by direct irradiation.

We then isolated µEV from *Abl-µNLS*-Abl^{WT} and *Abl-µNLS*-$Abl^{\mu NLS}$ MEFs and found comparable total protein and RNA content among several independent µEV preparations (Figure 6, A and B). The protein-to-particle ratios of µEV from these reconstituted *Abl-µNLS* MEFs were also comparable to those of EV from *Abl-wt* cells and µEV from parental *Abl-µNLS* cells (Figure 1G). The unirradiated responder MEFs internalized the µEVs from *Abl-µNLS*-Abl^{WT} *and Abl-µNLS*-$Abl^{\mu NLS}$ MEFs to a similar extent (Figure 6, C and D). Thus, expression of Abl^{WT} or $Abl^{\mu NLS}$ did not affect the overall production or the uptake ability of EV. Nevertheless, µEV-IR-Abl^{WT}, but not µEV-IR-$Abl^{\mu NLS}$, regained ROS-inducing activity (Figure 6, E and F). Because nuclear entry of wild-type Abl protein was sufficient to correct the ROS-induction defect of µEV-IR, these results established that nuclear Abl is required for irradiated cells to produce EV-IR with ROS-inducing activity.

Abl kinase activity required for irradiated cells to produce reactive oxygen species–inducing EV-IR

Ionizing radiation not only induces Abl nuclear accumulation but also activates Abl kinase activity (Baskaran *et al.*, 1997; Kaidi and Jackson, 2013). To assess the role of Abl kinase, we pretreated MEFs with the Abl kinase inhibitor imatinib before irradiation (Figure 7A) to generate EV-(IM+IR). We found that the ROS-inducing activity of EV-(IM+IR) was significantly reduced when compared with that of EV-IR (Figure 7, B and C), suggesting a requirement for Abl kinase in the production of EV-IR with ROS-inducing activity.

Because imatinib is a selective but not a specific inhibitor of Abl kinase, we further investigated the kinase requirement by stably expressing a kinase-defective (KD) Abl^{KD} (with K290H substitution to disrupt ATP binding) through retrovirus-mediated gene transfer to generate *Abl-µNLS*-Abl^{KD} MEFs (Figure 7D). Irradiation induced nuclear accumulation of Abl in *Abl-µNLS*-Abl^{KD} MEFs (Figure 7, E and F), consistent with previous findings that kinase activity is not necessary for Abl nuclear import. The *Abl-µNLS*-Abl^{KD} cells produced µEV-C-Abl^{KD} and µEV-IR-Abl^{KD} with protein content similar to that of those from *Abl-µNLS*- Abl^{WT} cells (Figure 7G). The µEV-C-Abl^{KD} and µEV-IR-Abl^{KD} were internalized by unirradiated MEFs with efficiencies similar to those from *Abl-µNLS*-Abl^{WT} cells (Figure 7, H and I).

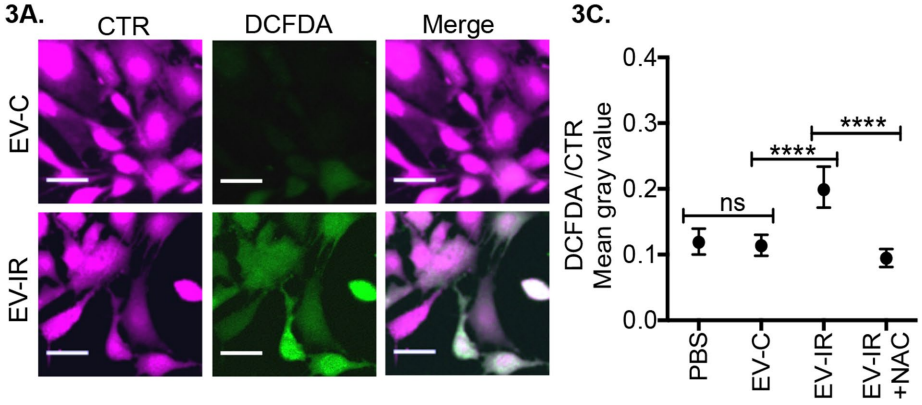

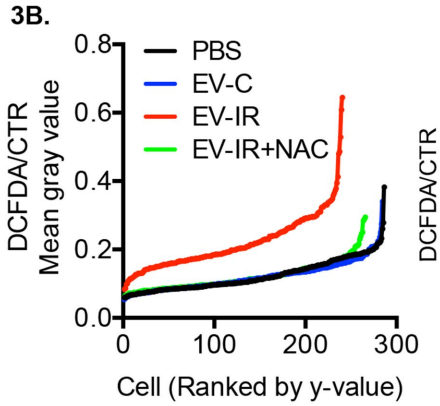

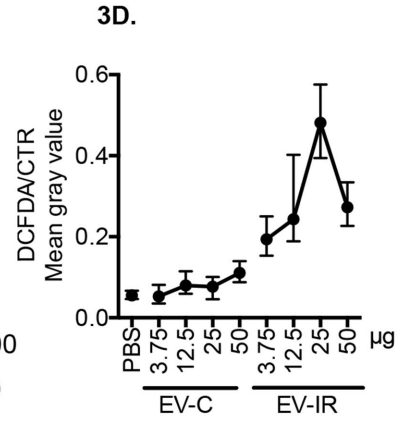

3E.

Treatments (24 hours)	Survival fractions (Colonies/ 1000 cells)	Relative DCFDA/ CTR ratios
PBS	43/1000	1
EV-C	48/1000	1.2
EV-IR	3/1000	3.2
Proteinase K treated EV-IR	5/1000	2.5
RNase A treated EV-IR	4/1000	2.7

FIGURE 3: (A–C) EV-IR but not EV-C increased ROS. (A) Representative images of live cells stained with cell-tracker red: CTR (magenta) and DCFDA (green) at 24 h after addition of EV-C or EV-IR (3.5 µg; scale bar 35 µm). (B) Values of DCFDA/CTR ratios of individual cells at 24 h after the indicated treatment from one representative experiment. NAC: N-acetylcysteine (5 mM). EV-C or EV-IR: 3.5 µg. (C) Medians with interquartile ranges of DCFDA/CTR ratios from three independent experiments with at least 200 cells analyzed per sample per experiment. ns, not significant, ****$P \leq 0.0001$, Kruskal–Wallis test. (D) EV-IR dose dependency in ROS induction: responder MEFs were treated with the indicated amounts of EV-C or EV-IR for 24 h and the ROS measured. Values shown are the medians and interquartile ranges of DCFDA/CTR ratios from two independent experiments with at least 200 cells analyzed per sample per experiment. (E) Protease or RNase treatment of EV-IR did not abolish BE. EV-IR were incubated with proteinase K (0.05 mg/ml, 10 min at 60°C) or RNaseA (0.5 mg/ml, 20 min at 37°C) before being added to responder MEFs.

However, µEV-IR-Abl^{KD} cells failed to induce ROS when added to unirradiated MEFs (Figure 7, J and K). Together, these results show that radiation-induced Abl nuclear localization and kinase activity are both required for irradiated cells to produce EV-IR with ROS-inducing activity.

Nuclear Abl-dependent miR-34c increase in EV-IR and EV-IR–treated cells

Ionizing radiation stimulates the expression of many microRNAs, including miR-34c, in directly irradiated cells (He *et al.*, 2007; Chaudhry, 2014). We have previously shown that nuclear Abl stimulates the biogenesis of miR-34c in DNA damage response (Tu *et al.*, 2015). A recent study found that the majority of intracellular microRNAs are present in EV produced by cultured cells (Shurtleff *et al.*, 2016). We therefore tested the hypothesis that nuclear Abl-dependent and radiation-induced increase in miR-34c may raise the levels of miR-34c in EV-IR.

As would be predicted, intracellular miR-34c levels were higher in irradiated (IR) than control (Con) MEFs (Figure 8A). This IR-induced increase in miR-34c was lower in *Abl-µNLS* than in *Abl-wt* MEFs (Figure 8, A and B) and the expression of Abl^{WT} enhanced the -34c induction by IR (Figure 8, B and C). With the EV preparations from *Abl-wt* MEFs, we found higher levels of miR-34c in EV-IR than in EV-C (Figure 8D). However, µEV-IR from *Abl-µNLS* MEFs did not contain higher levels of miR-34c than µEV-C (Figure 8E). Expression of Abl^{WT} in *Abl-µNLS* MEFs restored the miR-34c increase in µEV-IR-Abl^{WT} relative to µEV-C-Abl^{WT} (Figure 8F), although the relative abundance of miR-34c was only twofold higher in µEV-IR-Abl^{WT} relative to µEV-C-Abl^{WT} and significantly lower than the 20-fold difference between EV-IR and EV-C (compare Figure 8D to Figure 8F). This partial rescue of miR-34c levels in µEV-IR-Abl^{WT} was likely to be due to the lower- than-endogenous levels of exogenous Abl^{WT} in the reconstituted *Abl-µNLS*-Abl^{WT} MEFs (Figure 5B).

We also measured the levels of miR-34c in the unirradiated responder MEFs after incubations with EV. We found a twofold increase in miR-34c in responder cells after treatment with EV-IR, but not EV-C (Figure 8G). Treatment with µEV-C or µEV-IR, however, did not raise the intracellular miR-34c levels in responder cells (Figure 8H). Expression of Abl^{WT} in *Abl-µNLS* MEFs not only raised miR-34c levels in µEV-IR-Abl^{WT} (Figure 8F) but also restored the miR-34c increase in µEV-IR-Abl^{WT}–treated responders (Figure 8I). Together, these results showed that nuclear Abl is required to raise the miR-34c levels in EV-IR and that treatment with EV-IR raised the intracellular miR-34c levels in unirradiated responder cells. In addition, these results showed a correlation between the miR-34c levels and the ROS-inducing activities of EV.

EV-miR34c from unirradiated cells and miR-34c-mimic induce reactive oxygen species

To determine whether it is possible to program EV from unirradiated cells to induce ROS, we overproduced miR-34c in HEK293T cells, which have been shown to secrete the majority of intracellular miR in EV (Shurtleff *et al.*, 2016). Transfections of HEK293T cells with the vector miR-34c minigene (Figure 9A) and/or AblPPn (Figure 9B) did not alter the total protein (Figure 9C), RNA (Figure 9D), or protein-to-particle ratios (Figure 1G) of EV from HEK293T cells. However, transfection with the miR-34c minigene raised miR-34c levels in transfected cells and in EV-miR-34c isolated from the media of those cells compared with cells transfected with vector or AblPPn (Figure 9, E and F). Cotransfection of miR-34c minigene with AblPPn further increased the intracellular levels of miR-34c and resulted in higher levels of miR-34c in EV-miR-34c+AblPPn than in EV-miR-34c (Figure 9, E and F). When added to unirradiated responder MEFs, EV-miR-34c and EV-miR-34c+AblPPn increased the intracellular levels of miR-34c in proportion to those found in the EVs (Figure 9G). These results showed that ectopically expressed miR-34c was secreted in EV by unirradiated HEK293T cells and that the miR-34c levels in EV correlated with those in the producer cells and determined those in responder MEFs incubated with the HEK293T-EV.

We then measured ROS levels in responder MEFs after incubation with the HEK293T-EV preparations. We found that treatment with EV-miR-34c and EV-miR-34c+AblPPn, but not EV-vector or EV-AblPPn, raised ROS levels (Figure 9, H and I) that were proportional to the miR-34c levels in the responders (compare Figure 9I with Figure 9G). These results showed that irradiation is not required for HEK293T cells to produce miR-34c–containing EV with ROS-inducing activity. We also transfected unirradiated MEFs with miR-34c mimic to raise the intracellular levels of miR-34c (Figure 9, J and K) and found that transfection with the miR-34c mimic but not the control mimic could induce ROS in unirradiated responder MEFs without the need for EV addition (Figure 9, L and M). Taken together, results in Figure 9 show a quantitative correlation between miR-34c levels in EV and in EV-treated responder cells. Furthermore, these results show that miR-34c–containing EV from unirradiated cells can induce ROS and that ectopic expression of high levels of miR-34c can also induce ROS without added EV.

EV-IR from miR-34–family triple knockout mouse embryonic fibroblasts cannot induce reactive oxygen species

To determine whether endogenous miR-34c is necessary for ROS induction, we irradiated primary MEFs derived from the miR34-family (a/b/c) triple knockout (TKO) and littermate wild-type (WT) mice (Concepcion *et al.*, 2012; Figure 10A). We found that irradiation induced comparable levels of ROS in the *miR34*^{WT} and the *miR34*^{TKO} MEFs (Figure 10, B and C), showing that the endogenous miR-34a/b/c are not required for ROS induction by direct irradiation. We then isolated EV from irradiated *miR34*^{WT} and *miR34*^{TKO} MEFs (Figure 10D) and found similar protein content in those EV preparations (Figure 10E). When added to unirradiated responder MEFs, EV-IR-miR34^{WT} induced ROS (Figure 10, F and G), showing that EV-IR isolated from primary (*miR34*^{WT}) MEFs also had ROS-inducing activity. However, EV-IR-miR34^{TKO} failed to induce ROS in responder cells (Figure 10, F and G). As would be expected, treatment with EV-IR-miR34^{WT}, but not EV-IR-miR34^{TKO}, raised the intracellular levels of miR-34c in the unirradiated responder cells (Figure 10H). These results show that the miR-34 family of miR is required for irradiated cells to produce EV-IR with ROS-inducing activity.

EV treatment raised miR-34c and reactive oxygen species levels in *miR-34*^{TKO} mouse embryonic fibroblasts

To determine whether endogenous miR-34c is required for EV-IR to induce ROS, we treated unirradiated *miR34*^{TKO} MEFs with EV-C and EV-IR (from *Abl-wt* MEFs) and then measured ROS and miR-34c levels in these *miR34*^{TKO} cells (Figure 10I). We found that treatment of *miR34*^{TKO} MEFs with either EV-C or EV-IR led to a detectable increase in the intracellular levels of miR-34c, with EV-IR raising miR-34c more than EV-C (Figure 10L). Correlating with these increases in intracellular miR-34c, we found significantly higher levels of in ROS in EV-C– and EV-IR–treated *miR34*^{TKO} MEFs, with EV-IR–treated cells containing significantly higher levels of ROS than EV-C–treated cells (Figure 10, J and K). Because the *miR-34a/b/c* loci are knocked out in *miR34*^{TKO} cells, the EV-mediated increase in intracellular miR-34c (Figure 10L) could not have been derived from the endogenous locus. Thus, these results strongly suggest that EV can transfer exogenous miR-34c into unirradiated cells for ROS induction.

DISCUSSION

Extracellular vesicles from irradiated cells induce bystander effects

This study has established a role for extracellular vesicles (EV) in RIBE on colony formation and redox homeostasis. We show that IR does not have significant effects on the overall particle numbers, total protein, or RNA content of EV. However, IR can alter the biological activity of EV because EV-IR isolated from media of irradiated MEFs, but not EV-C from control MEFs, can induce ROS and inhibit colony formation in unirradiated MEFs. We also show that EV-IR-induced ROS contributes to colony inhibition because an anti-oxidant NAC neutralized the ROS and reduced the colony-inhibitory activity of EV-IR. A large number of previous studies have shown that conditioned media from irradiated cells contained ROS-inducing factors (Mladenov *et al.*, 2018). Our results suggest that at least one of those ROS inducers is present in the EV fraction of the conditioned media, thus supporting the concept that extracellular vesicles can transmit RIBE signals.

Nuclear Abl kinase requirement for production of extracellular vesicles with reactive oxygen species–inducing activity

Results from this study have uncovered a new function for nuclear Abl kinase in DNA damage response: it is required for irradiated cells to produce EV with ROS-inducing activity. Using MEFs with the *Abl-μNLS* allele created in our lab (Preyer *et al.*, 2007), we show that ROS induction in irradiated cells does not require nuclear localization of Abl. This is not a surprising observation, since IR-induced ROS occurs in the cytoplasm and involves the mitochondria (Leach *et al.*, 2001). However, we demonstrate here that nuclear Abl and its kinase activity are required for the production of RIBE-competent EV. Supporting this conclusion are the results that the Abl-genotypes did not affect the overall production of EVs, but μEV-IR from the *Abl-μNLS* MEFs could not induce ROS, and that expression of Abl^{WT}, but not Abl$^{\mu NLS}$ or Abl^{KD}, in the *Abl-μNLS* MEFs restored the ROS-inducing activity of μEV-IR. These experiments with the *Abl-μNLS* germline mutant established that nuclear Abl is nonessential for radiation to induce ROS, but nuclear Abl is essential for irradiated cells to produce EV with ROS-inducing activity.

Extracellular vesicle–mediated transfer of miR-34c

The concept that extracellular vesicles play a role in cell–cell communication by exchanging cellular contents is well established (Valadi *et al.*, 2007; Tkach and Thery, 2016). In this study, we show

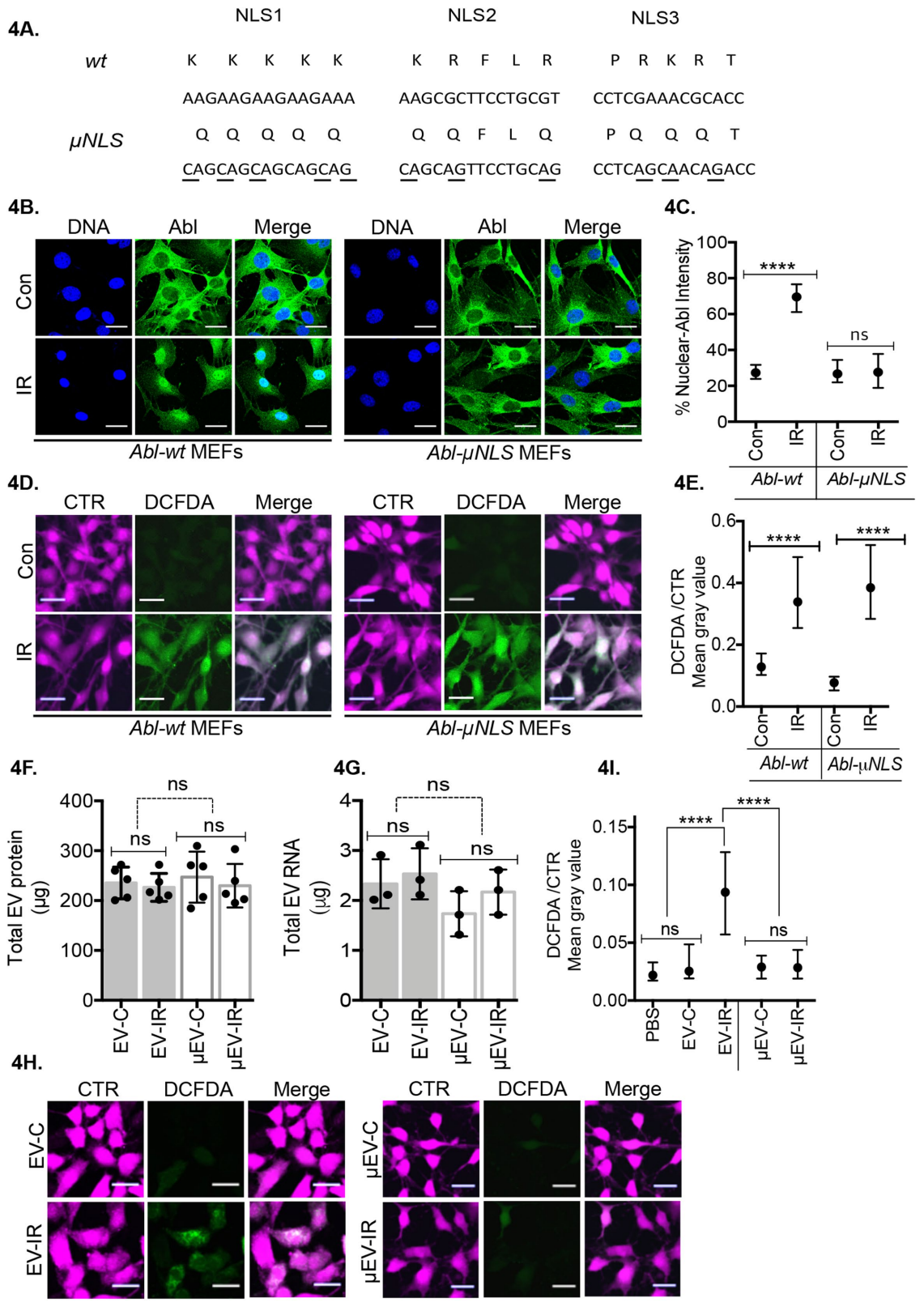

FIGURE 4: Extracellular vesicles from irradiated *Abl-μNLS* cells (μEV-IR) failed to induce ROS. (A) Substitution mutations of the three nuclear localization signals (NLS) in the *Abl-μNLS* allele. (B, C) Radiation-induced nuclear Abl accumulation: (B) representative immunofluorescence images of Abl (green) and DNA (blue) in the indicated MEFs: Con, no irradiation; IR: 3 h after 10 Gy (scale bar 35 μm). (C) Percent nuclear intensity of Abl in the indicated MEFs with no irradiation (Con) or irradiation (IR). Values shown are the medians and interquartile ranges from 20–30 cells per sample. ns, not significant, ****$P \leq 0.0001$, Kruskal–Wallis test. (D, E) Radiation-induced ROS: (D) representative images of indicated live cells stained with CTR (magenta) and DCFDA (green) 24 h after no irradiation (Con) or irradiation (IR, 10 Gy; scale bar 35 μm). (E) DCFDA/CTR ratios shown are the medians with interquartile ranges from two independent experiments with

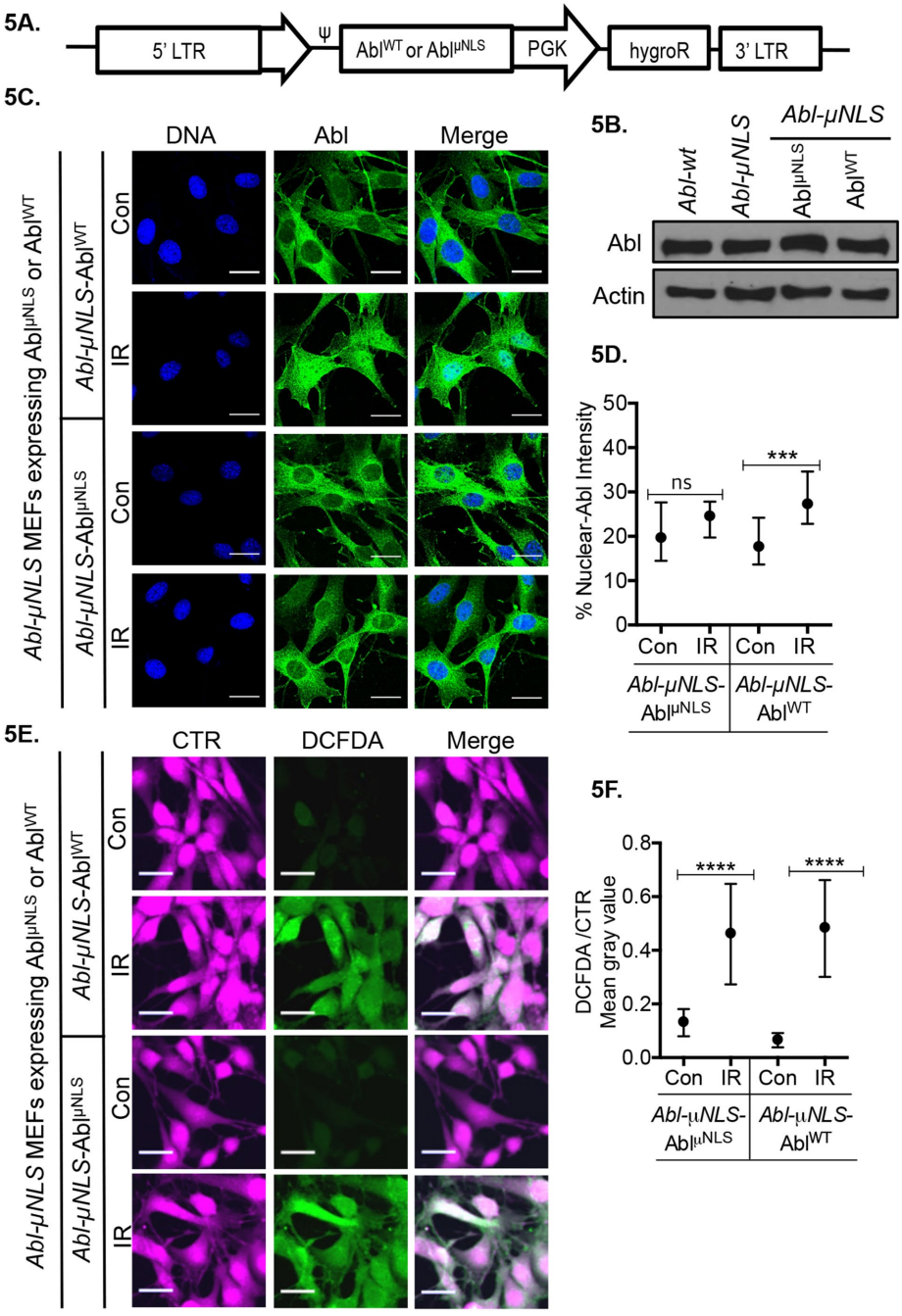

FIGURE 5: Expression of Abl^{WT} and Abl$^{\mu NLS}$ in *Abl-μNLS* MEFs. (A) Schematic of the pMSCV retroviral construct for expression of Abl^{WT} or Abl$^{\mu NLS}$. (B) Immunoblotting of Abl in whole lysates of the indicated cells. (C, D) Radiation effect on Abl localization: (C) representative immunofluorescence images of Abl (green) and DNA (blue) in *Abl-μNLS*-Abl^{WT} and *Abl-μNLS*-Abl$^{\mu NLS}$ MEFs: Con, no irradiation; IR: 3 h after 10 Gy (scale bar 35 μm). (D) Percent nuclear intensity of Abl in the indicated MEFs with no irradiation (Con) or irradiation (IR). Values shown are the medians and interquartile ranges from 20–30 cells per sample. ns, not significant, *** $P \leq 0.001$, Kruskal–Wallis test. (E, F) Radiation-induced ROS: (E) representative images of the indicated live cells stained with CTR (magenta) and DCFDA (green) at 24 h after no irradiation (Con) or 10 Gy IR (scale bar 35 μm). (F) DCFDA/CTR ratios shown are the medians with interquartile ranges from two independent experiments with at least 200 cells analyzed per sample per experiment. **** $P \leq 0.0001$, Kruskal–Wallis test.

that treatment with EV-IR from irradiated MEFs, or with EV-miR-34c from miR-34c-minigene–transfected but unirradiated HEK293T cells, can increase the levels of miR-34c in unirradiated responder cells. Our results showed a quantitative correlation between the levels of miR-34c in EV and those in EV-treated responder cells. Furthermore, we show that treatment with EV-IR led to miR-34c increase in the *miR34*^{TKO} MEFs that lacked the endogenous *miR-34c* gene. These results strongly support the conclusion that miR-34c can be transferred from cell to cell via EV. However, we cannot rule out the possibility that EV-IR may also induce the expression of endogenous miR-34c. Because EV-IR transfers miR-34c to increase ROS that may damage DNA, it is conceivable that the exogenous miR-34c-induced ROS may activate DDR in unirradiated cells to stimulate expression of the endogenous miR-34c and thus amplify and spread EV-miR-34c–mediated bystander effects.

ROS induction by miR-34c

In previous studies, we have established that nuclear Abl is required for the expression of p53-target genes in DDR to induce apoptosis (Gong *et al.*, 1999; Sridevi *et al.*, 2013) and for the processing of p53-induced *pre-miR-34c* (Tu *et al.*, 2015). Because miR-34c is not essential to DDR-induced apoptosis (Concepcion *et al.*, 2012), we searched for alternative functions for miR-34c in DDR and found that nuclear Abl-dependent and IR-induced miR-34c

at least 200 cells analyzed per sample per experiment. **** $P \leq 0.0001$, Kruskal–Wallis test. (F) Total protein in μEV-C or μEV-IR isolated from media of unirradiated (C) and irradiated (IR) *Abl-μNLS* MEFs compared with total protein in EV-C or EV-IR isolated from media of *Abl-wt* MEFs. Values shown are mean ± SD from five independent EV preparations. ns, not significant, one-way ANOVA. (G) Total RNA in the indicated EV. Values shown are mean ± SD from three independent EV preparations. ns, not significant, one-way ANOVA. (H, I) EV-induced ROS: (H) representative images of live responder MEFs (unirradiated *Abl-wt*) stained with the indicated dyes at 24 h after treatment with 3.5 μg each of the indicated EV (scale bar 35 μm). (I) DCFDA/CTR ratios shown are the medians with interquartile ranges from three independent experiments with at least 200 cells analyzed per sample per experiment. ns, not significant, **** $P \leq 0.0001$, Kruskal–Wallis test.

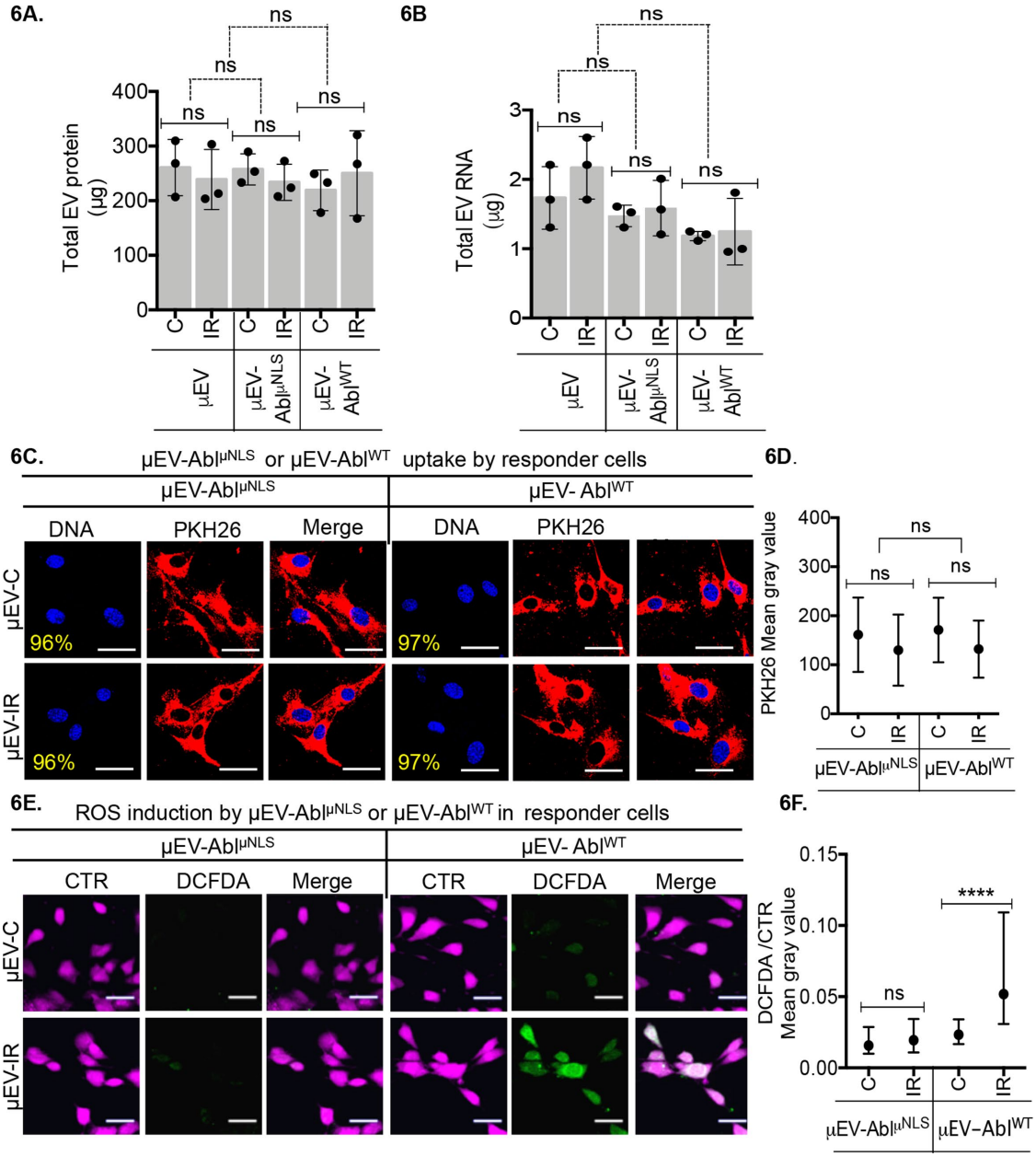

FIGURE 6: Expression of Abl^{WT} but not Abl$^{\mu NLS}$ restored ROS-inducing activity to µEV-IR. (A) Total protein in the indicated µEV, µEV-Abl$^{\mu NLS}$, and µEV-Abl^{WT} preparations from 100 ml media conditioned by *Abl-µNLS*, *Abl-µNLS*-Abl$^{\mu NLS}$, or *Abl-µNLS*-Abl^{WT} MEFs. C: no irradiation, IR: 10 Gy irradiation. Values shown are mean ± SD from three independent EV preparations. ns, not significant, one-way ANOVA. (B) Total RNA in the indicated µEV from 100 ml conditioned media from the indicated MEFs. Values shown are mean ± SD from three independent EV preparations. ns, not significant, one-way ANOVA. (C, D) Uptake of PKH26-labeled µEV by unirradiated MEFs: (C) representative images (scale bar 35 µm) with the percentage of responder cells stained positive for the indicated PKH26-µEV at 24 h after µEV addition. (D) Quantification of PKH26 mean gray values in cells treated with the indicated PKH26-µEV (25 µg each). The mean ± SD from at least six images are shown. ns, not significant, one-way ANOVA. (E, F) µEV-induced ROS: (E) representative images of live responder cells treated with the indicated µEV preparations (3.5 µg each) and stained with CTR (magenta) plus DCFDA (green) at 24 h after µEV addition (scale bar 35 µm). (F) DCFDA/CTR ratios shown are medians with interquartile ranges from three independent experiments with at least 200 cells analyzed per sample per experiment. ns, not significant, ****$P \leq 0.0001$, Kruskal–Wallis test.

expression is required for increasing the miR-34c levels in EV-IR for transfer into unirradiated cells to induce ROS. We show that EV-IR from *miR34*^{TKO} MEFs cannot induce ROS. We also show that EV-miR34c produced by unirradiated cells and transfection with miR-34c mimic without EV addition are each sufficient to induce ROS. These results suggest a novel function for miR-34c in radiation-induced bystander oxidative stress.

It is of interest to note that neither nuclear Abl nor the miR-34 family of microRNAs are required for irradiation to induce ROS, but nuclear Abl and the miR-34 family are both required for transmission

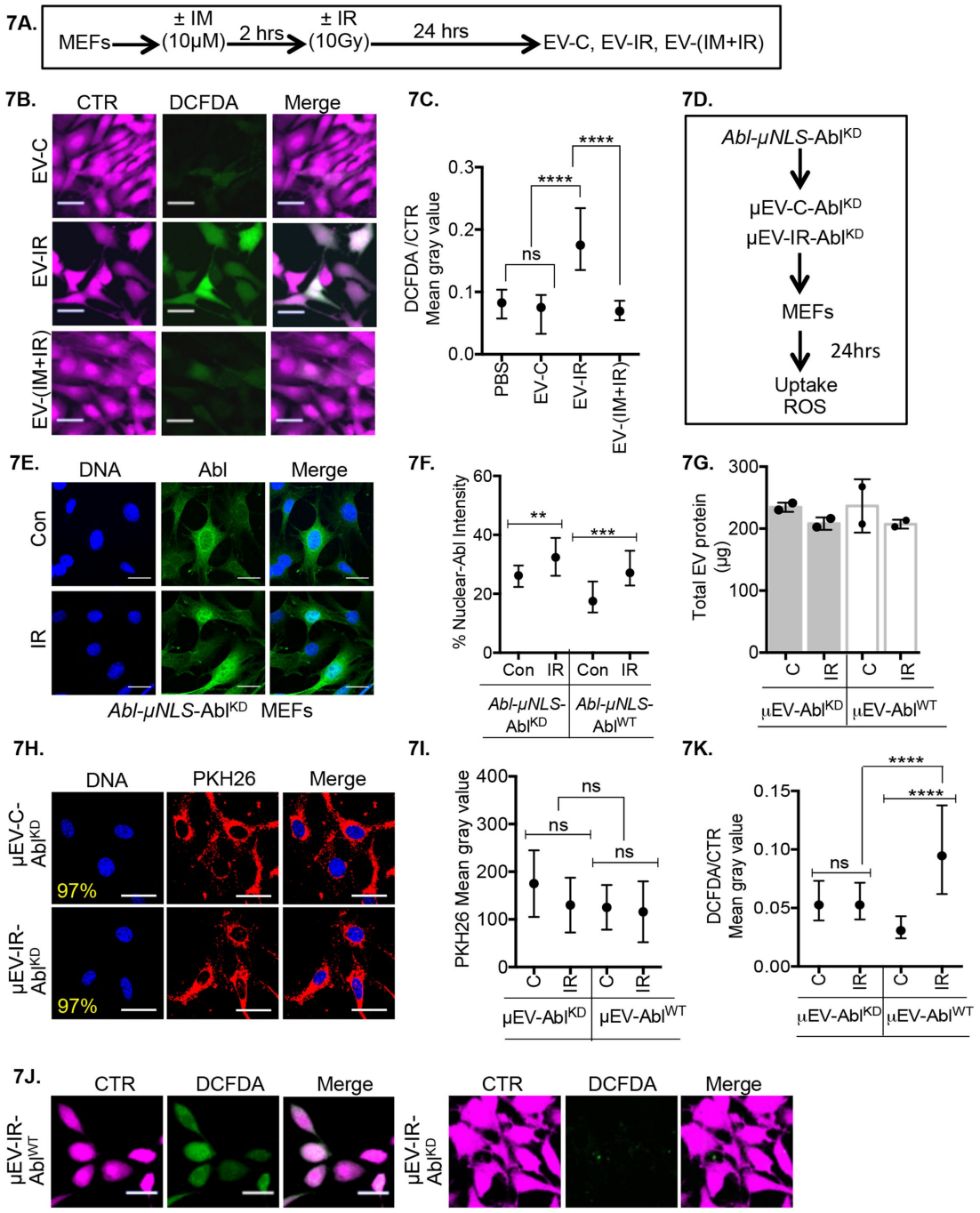

FIGURE 7: Abl kinase required for irradiated cells to produce EV-IR with ROS-inducing activity. (A) Timeline of Imatinib (IM) treatment. (B, C) EV-induced ROS: (B) representative images of live responder cells treated with the indicated EV and stained with CTR (magenta) and DCFDA (green) at 24 h after EV addition (scale bar 35 μm). (C) DCFDA/CTR ratios shown are medians with interquartile ranges from three independent experiments with at least 200 cells analyzed per sample per experiment. ns, not significant, $^{****}P \leq 0.0001$, Kruskal–Wallis test. (D) Summary of experiments with *Abl-μNLS*-Abl^{KD} MEFs. (E, F) Radiation-induced nuclear Abl: (E) representative immunofluorescence images of Abl (green) and DNA (blue) in the indicated MEFs: Con, no irradiation; IR: 3 h after 10 Gy (scale bar 35 μm). (F) Percent nuclear intensity of Abl in the indicated MEFs with no irradiation (Con) or irradiation (IR). Values shown are the medians and interquartile ranges from 20–30 cells per sample. $^{**}P \leq 0.01$, $^{***}P \leq 0.001$, Kruskal–Wallis test. (G) Total protein in μEV isolated from 100 ml media conditioned by *Abl-μNLS*-Abl^{KD} (μEV-C-Abl^{KD}, μEV-IR-Abl^{KD}) or *Abl-μNLS*-Abl^{WT} (μEV-C-Abl^{WT}, μEV-IR-Abl^{WT}) MEFs. (H, I) Uptake of PKH26-labeled μEV by unirradiated MEFs: (H) representative images (scale bar 35 μm) with the percentage of cells stained positive for the indicated PKH26-μEV at 24 h after μEV addition. (I) Quantification of PKH26 mean gray values in MEFs treated with the indicated PKH26-μEV. The mean and SD from at least six images are shown. ns, not significant, one-way ANOVA. (J, K) μEV-induced ROS: (J) representative images of live responder cells treated with the indicated μEV preparations and stained with CTR (magenta) plus DCFDA (green) at 24 h after μEV addition (scale bar 35 μm). (K) DCFDA/CTR ratios shown are medians with interquartile ranges from one independent experiment with at least 200 cells analyzed per sample per experiment. ns: not significant, $^{****}P \leq 0.0001$, Kruskal–Wallis test.

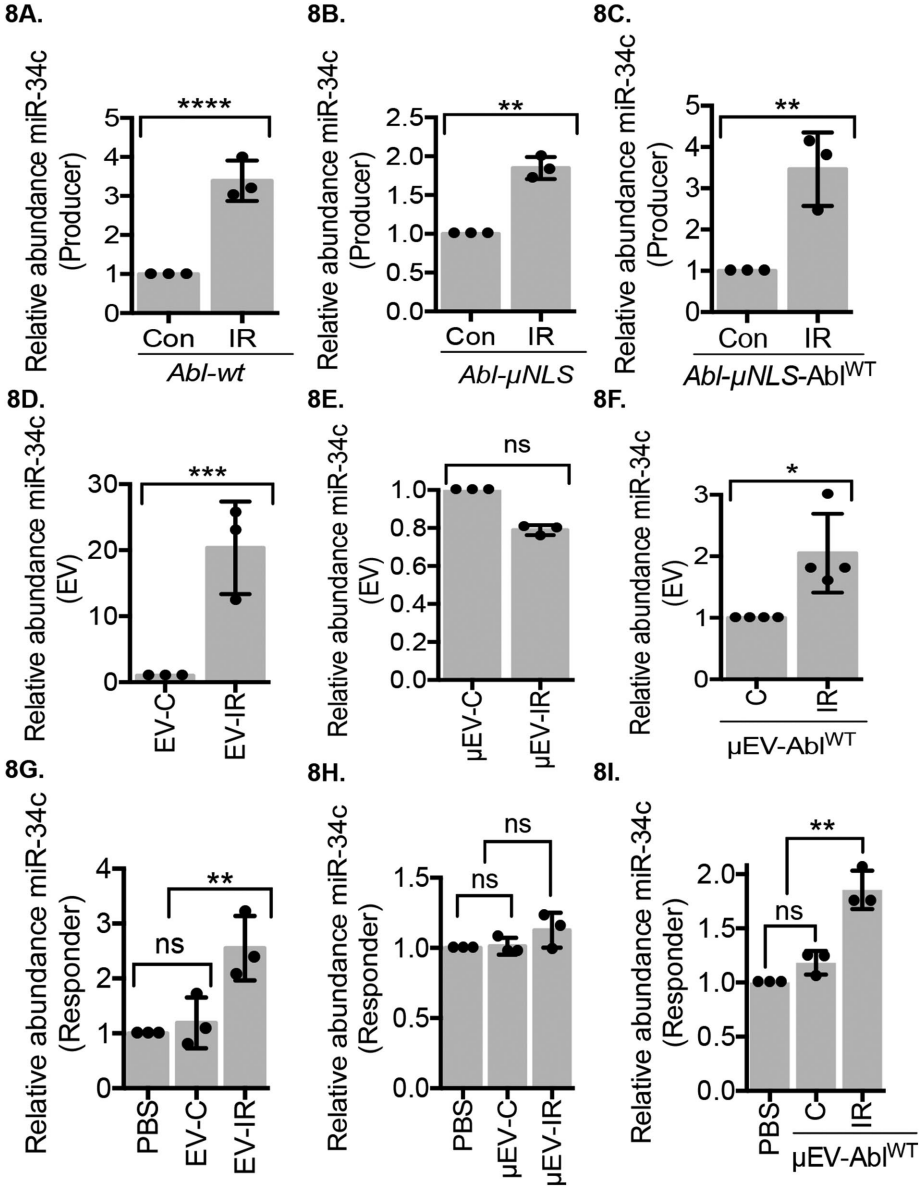

FIGURE 8: Radiation-induced and nuclear Abl-dependent increase of miR-34c in irradiated cells, EV-IR, and EV-IR-treated cells. (A–C) Radiation-induced miR-34c: *Abl-wt* (A), *Abl-μNLS* (B), and *Abl–μNLS*-Abl^{WT} MEFs (C) were unirradiated (Con) or irradiated (IR, 10 Gy, 24 h) and the relative abundance of miR-34c in total cellular RNA quantified and with each Con sample set to 1. Values shown are mean ± SD from three independent experiments. $^{**}P \le 0.01$, $^{****}P \le 0.0001$, one-way ANOVA. (D–F) miR-34c levels in EV. Relative abundance of miR-34c in total RNA extracted from the indicated EV: (D) EV-C, EV-IR from *Abl-wt* MEFs, (E) μEV-C, μEV-IR from *Abl-μNLS* MEFs, (F) μEV-C-Abl^{WT}, μEV-IR-Abl^{WT} from *Abl-μNLS*-Abl^{WT} MEFs. Values shown are mean ± SD from three independent experiments with each control EV set to 1. ns, not significant, $^{*}P \le 0.05$, $^{***}P \le 0.001$, one-way ANOVA. (G–I) miR-34c levels in EV-treated responder cells: unirradiated responder cells (*Abl-wt* MEFs) treated with PBS or the indicated EV (25 μg): (G) EV-C, EV-IR, (H) μEV-C, μEV-IR, and (I) μEV-C-Abl^{WT}, μEV-IR-Abl^{WT} were harvested at 24 h and the relative abundance of miR-34c in total cellular RNA quantified with each PBS-treated sample was set to 1. Values shown are mean ± SD from three independent experiments. ns: not significant, $^{**}P \le 0.01$, one-way ANOVA.

of the ROS response to bystander cells. While our results have established a role for miR-34c in the induction of ROS, they do not exclude the possibility that EV-IR may also directly transfer ROS from irradiated cells to bystander cells. However, if a direct transfer of ROS by EV-IR were to exist, our results suggest that such a direct ROS transfer by EV must still require both the nuclear entry of Abl and the miR-34 family of microRNAs.

Previous studies have found that exposure to IR causes the intracellular abundance of many microRNAs to increase (He *et al.*, 2007; Mao *et al.*, 2014), and these IR-inducible microRNAs may affect an array of cellular responses to radiation (Chaudhry, 2014). We show here for the first time that IR-induced miR-34c is secreted in extracellular vesicles for transfer into unirradiated cells to cause oxidative stress. Computational analyses have predicted hundreds of miR-34c target genes that might collectively be involved in the observed induction of ROS. However, it is also possible that miR-34c may trigger a cascade of gene expression alterations beyond the computationally predicted targets to increase ROS. Identification of the relevant miR-34c target genes in RIBE awaits future investigation.

MATERIALS AND METHODS

Cell lines

Fibroblasts were derived from *Abl*$^{+/+}$ (*Abl-wt*) or littermate *Abl*$^{\mu/\mu}$ (*Abl-μNLS*) mouse embryos. The *Abl-μNLS* allele was generated by knock-in mutations to replace the 11 lysines and arginines in the three nuclear localization signals (NLS) with glutamine (Preyer *et al.*, 2007). The *Abl-wt* and *Abl-μNLS* MEFs were immortalized by serial passages, and these MEFs do not express p53. Primary, nonimmortalized MEFs from *miR-34a/b/c*-triple knockout mice (miR34^{TKO}) and wild-type littermates (miR34^{WT}; (Concepcion *et al.*, 2012) were irradiated between passages 3 and 6. MEFs and HEK293T cells (Thermo Fisher Scientific) were cultured in DMEM high-glucose with 10% fetal bovine serum (FBS) and antibiotics.

Irradiation

Cells were exposed to 10 Gy of gamma irradiation using a Mark I Model 50 irradiator with cesium 137 isotope as source (J.L. Shepherd & Associates).

Isolation of extracellular vesicles

To isolate EV from MEFs, two batches of 10^7 cells (in 10 10-cm dishes) were switched to FBS-free media with 1% bovine serum albumin (BSA) 2 h before transfer to the radiation facility, where one batch was irradiated while the other batch was not irradiated (unirradiated). At 24 h after radiation, the conditioned media (CM) were collected for EV isolation by differential ultracentrifugation as previously described (Thery *et al.*, 2006; Figure 1A). The pelleted EV fraction was washed and resuspended in 300 μl of phosphate-buffered saline (PBS) and stored in 50-μl aliquots at –80°C.

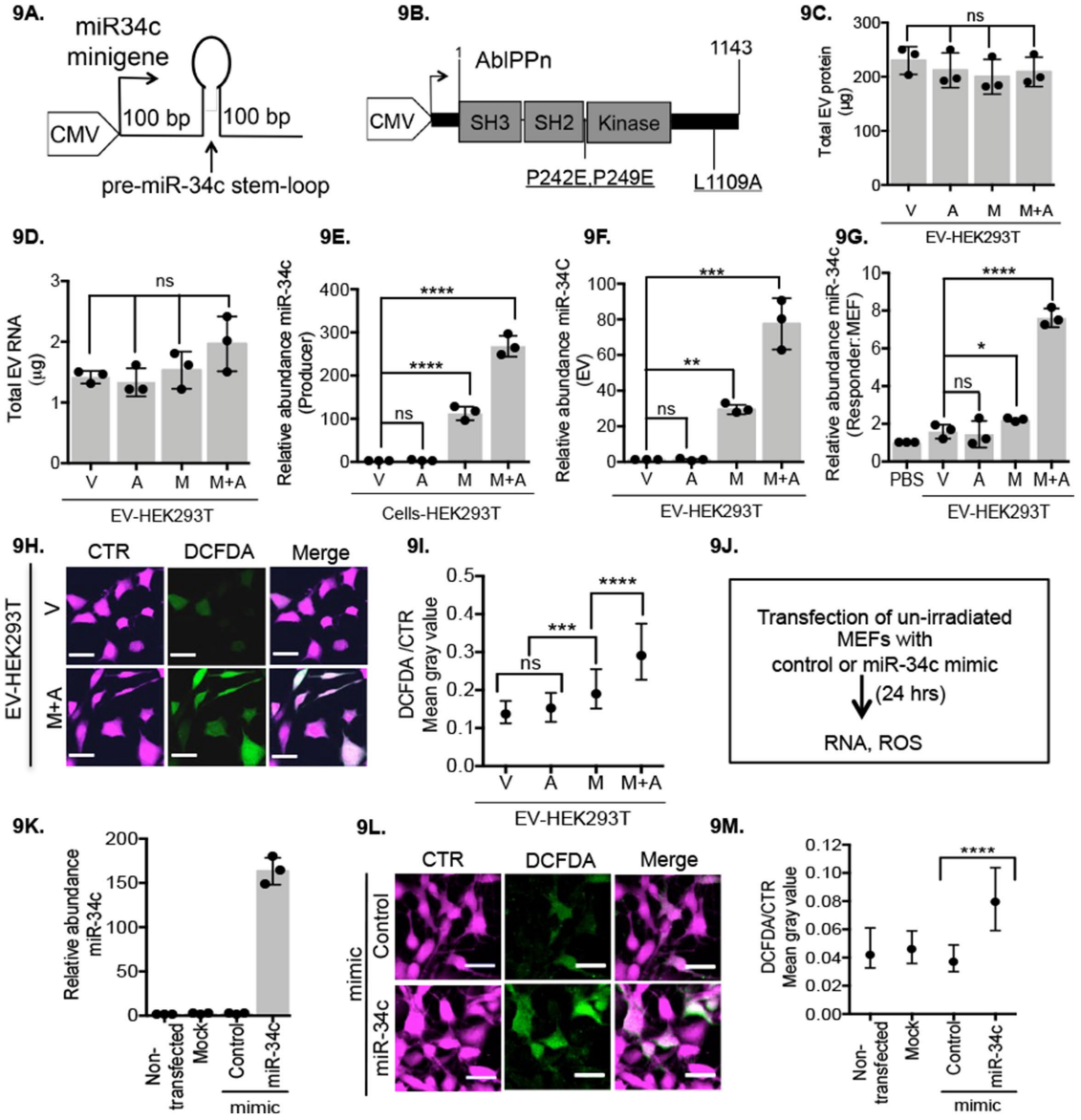

FIGURE 9: ROS induction by EV-miR-34c from unirradiated cells and by transfection with miR-34c mimic. (A, B) Schematics of the miR-34c-minigene and the AblPPn expression constructs. (C) Total protein in EV isolated from 100 ml of media conditioned by HEK293T cells (EV-HEK293T) transfected with Vector (V), AblPPn (A), miR-34c minigene (M), or miR-34c minigene and AblPPn (M+A). Values shown are mean ± SD from three independent EV preparations. ns: not significant, one-way ANOVA. (D) Total RNA in the indicated EV, each from 100 ml of media. Values shown are mean ± SD from three independent EV preparations. ns: not significant, one-way ANOVA. (E–G) Relative abundance of miR-34c in (E) unirradiated HEK293T cells transfected with the indicated plasmid DNA, with normalized abundance of miR-34 in vector (V)-transfected cells set to 1; (F) EV from transfected HEK293T cells with normalized miR-34c abundance in EV-vector (V) set to 1; (G) unirradiated MEFs after treatments with the indicated EV (25 µg each) from transfected HEK293T cells with normalized miR-34c abundance in PBS-treated MEFs set to 1. Values shown are mean ± SD from three independent experiments. ns: not significant, $^{**}P \leq 0.01$, $^{***}P \leq 0.001$, $^{****}P \leq 0.0001$, one-way ANOVA. (H, I) EV-miR-34c induced ROS: (H) representative images of live responder cells treated with the indicated EV preparations and stained with CTR (magenta) plus DCFDA (green) at 24 h after EV addition (scale bar 35 µm). (I) DCFDA/CTR ratios shown are medians with interquartile ranges from three independent experiments with at least 200 cells analyzed per sample per experiment. ns: not significant, $^{***}P \leq 0.001$, $^{****}P \leq 0.0001$, Kruskal–Wallis test. (J) Timeline of miR mimic transfection experiment. (K) Relative abundance of miR-34c in transfected MEFs at 24 h after transfection with no RNA (mock) or control or miR-34c mimic. Normalized miR-34c abundance in nontransfected cells was set to 1. Values shown are mean ± SD from three technical repeats. (L, M) miR-34c-mimic induced ROS: (L) representative images of live responder cells stained with CTR (magenta) and DCFDA (green) at 24 h after transfection with control or miR-34c mimic (scale bar 35 µm). (M) DCFDA/CTR ratios shown are medians with interquartile ranges from 400 cells per sample. $^{****}P \leq 0.0001$, Kruskal–Wallis test.

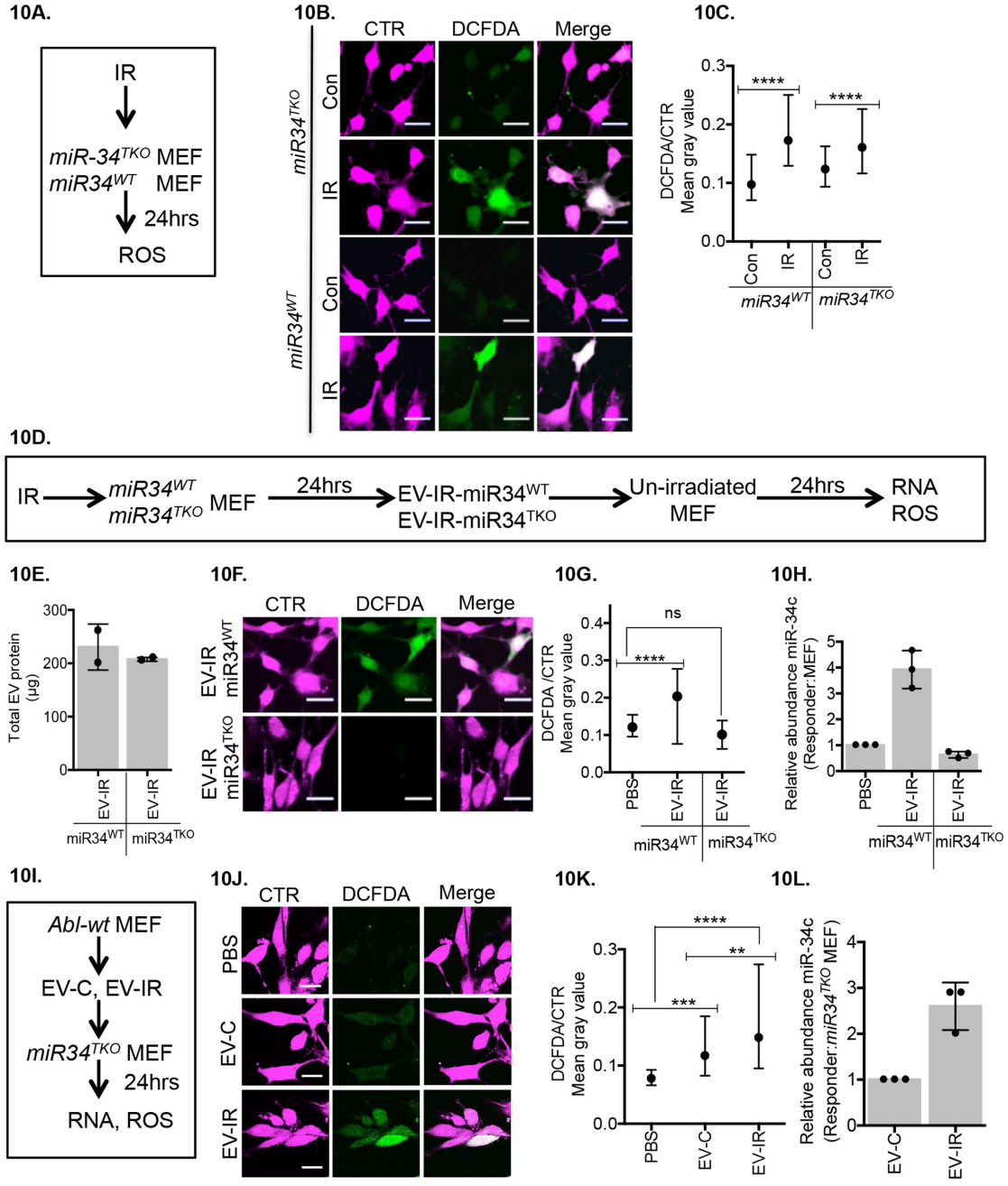

FIGURE 10: Experiments with *MiR34*^{TKO} MEFs. (A) Timeline of irradiation of primary MEFs from *miR34*^{WT} and *miR34*^{TKO} mice. (B, C) Radiation-induced ROS: (B) representative images of indicated live cells stained with CTR (magenta) and DCFDA (green) at 24 h after no irradiation (Con) or irradiation (IR, 10Gy; scale bar 35 µm). (C) DCFDA/CTR ratios shown are the medians with interquartile ranges from one experiment with at least 200 cells analyzed per sample per experiment. ****$P \leq 0.0001$, Kruskal–Wallis test. (D) Timeline of experiment with EV-IR from *miR34*^{WT} and *miR34*^{TKO} MEFs. (E) Total protein in EV-IR isolated from 100 ml media conditioned by irradiated *miR34*^{WT}and *miR34*^{TKO} MEFs. Values shown are mean ± SD from two independent EV preparations. (F, G) EV-IR from *miR34*^{TKO} MEFs failed to induce ROS: (F) representative images of live responder cells (unirradiated *Abl-wt* MEFs) stained with CTR (magenta) and DCFDA (green) after 24 h of treatment with the indicated EV-IR (25 µg each; scale bar 35 µm). (G) Values shown are medians with interquartile ranges from two independent experiments with at least 200 cells analyzed per sample per experiment. ns, not significant, ****$P \leq 0.0001$, Kruskal—Wallis test. (H) Relative abundance of miR-34c in responder cells treated with the indicated EV-IR (25 µg each) with normalized miR-34c abundance in PBS-treated responder cells set to 1. Values shown are mean ± SD from three technical repeats. (I) Timeline of experiment with unirradiated *miR34*^{TKO} MEFs as responder cells. (J, K) EV-IR–induced ROS in *miR34*^{TKO} MEFs: (J) representative images of live *miR34*^{TKO} MEFs stained with CTR (magenta) and DCFDA (green) at 24 h after treatment with EV-C or EV-IR from *Abl-wt* MEFs (25 µg each). (K) DCFDA/CTR ratios shown are medians with interquartile ranges from one experiment with at least 200 cells analyzed per sample. **$P \leq 0.01$, ***$P \leq 0.001$, ****$P \leq 0.0001$, Kruskal–Wallis test. (L) Relative abundance of miR-34c in *miR34*^{TKO} MEFs after 24 h of treatment with EV-C or EV-IR (25 µg) with normalized miR-34c abundance in EV-C–treated cells was set to 1. Values shown are mean ± SD from three technical repeats.

For isolation of EV from HEK293T cells, supernatant-1 collected after the 2000 × *g* spin (Figure 1A) was filtered through a 0.45-µm filter (Corning) before continuing to the next steps of ultracentrifugation. Protein content of EV was determined by the Lowry method.

Nanoparticle tracking analysis

Nanosight LM-10HS was used for nanoparticle tracking analysis. This analysis uses diffraction measurement of the Brownian motion of particles. The EV suspension was diluted 300-fold in PBS and 1 µl of the diluted suspension was videotaped by Nanosight to determine the size distribution and the concentration of particles. Each EV preparation was analyzed in triplicate as previously described (Akers *et al*., 2016).

Uptake of extracellular vesicles

EV suspensions were incubated with PKH26, a fluorescent membrane-binding dye (Sigma Aldrich), for 5 min at room temperature, followed by addition of 1% BSA, and then centrifuged at 100,000 × *g* for 70 min to isolate PKH26-labeled EV as previously described (Mineo *et al*., 2012). Responder MEFs were incubated with PKH26 in PBS or PKH26-labeled EV-C or PKH26-labeled EV-IR (25 µg each). After 3 or 24 h, cells were fixed with 4% *para*-formaldehyde (PFA) for 20 min at room temperature and counterstained with Hoechst 33342. Cells were viewed using an Olympus FV1000 Spectral Confocal microscope at 40× objective with images taken at 1024 × 1024 (Figure 1E), and using Leica TCS SP5 at 60× objective with images taken at 512 × 512 (Figures 6C and 7H). No fluorescence was detected in cells incubated with PKH in PBS. Using FIJI (ImageJ), we measured the total PKH26 mean gray value per image and calculated the mean and SD from at least six images per sample. The number of PKH26-positive cells per image was counted by eye, and the percentage was calculated from PKH26-positive cells over the total number of nuclei from at least six images per sample.

Colony formation assay

Responder cells (*Abl-wt* MEFs) were seeded at 1000 cells per 6-cm plate. Media were changed to 1% BSA without FBS before incubation with EV. After 24 h, cells were switched back to media with 10% FBS and cultured for 15 d with media refreshed every other day. The colonies were fixed with 100% methanol and stained with 0.05% crystal violet. Excess dye was removed, and plates were left to dry overnight. Clusters of more than 50 cells were considered as colonies. Survival fraction was calculated as colonies/cells seeded, with the survival fraction in PBS-treated plates set to 1. Images of the colonies were acquired using an Alpha imager HP System.

Reactive oxygen species assay

ROS was measured using the ROS-ID kit (Enzo Life Sciences) according to the manufacturer's protocol. Live cells were also stained with Cell Tracker Red (CTR; Molecular Probes) as a control for cell volume. Responder cells were seeded into chamber slides, incubated for 24 h with EV in media +1% BSA, stained with CTR (1:500, 30 min in media) followed by DCFDA (1: 5000, 45 min in PBS), washed with PBS, and then imaged. Live cell images were captured using an Olympus FV1000 spectral confocal microscope for CTR (Channel 3) and DCFDA (Channel 1). FIJI (ImageJ) software was used to create masks from channel 3 (CTR), and then the masks were transferred onto channel 1 (DCFDA). The mean gray values (MGVs) in channels 1 and 3 were recorded within the masks, and the DCFDA/CTR MGV ratio was calculated for each mask. See Figure 3B for plots of ranked DCFDA/CTR ratios of individual cells from representative experiments. From each experiment, we collected the ratios from at least 200 cells per sample. We then determined the median and the interquartile range of ratios collected from one to three experiments (200–600 cells) as indicated in the figure legends.

Immunofluorescence

Acid-washed coverslips stored in 100% ethanol were placed in 24-well plates, and ~20,000 MEFs were seeded per well. After incubation with EV for 24 h in serum-free media containing 1% BSA, cells were fixed in 4% PFA for 15 min, washed with 0.02% Tween-20 in Tri-buffered saline (TBS) twice (5 min each), permeabilized with 1% Triton X-100 in TBS for 15 min, and then blocked with 5% BSA for 30 min at room temperature. The coverslips were incubated with primary antibody for 1 h at 37°C: anti-Abl (8E9; 6 µg/ml) from Thermo Fisher Scientific. Coverslips were washed twice with 0.02% Tween-20 in TBS twice (5 min each) and then incubated with ALEXA fluor-488 (Invitrogen)-chicken anti-mouse (1/500) for 30 min. Nuclei were stained with Hoechst 33342. Coverslips were mounted with Prolong Gold Antifade Reagent and sealed with nail polish before imaging. Images were captured using an Olympus FV1000 spectral confocal microscope.

Quantification of nuclear Abl

Using the Analyze Particle (AP) tool in FIJI (ImageJ), nuclear masks were generated from Hoechst images. The nuclear masks were transferred to the corresponding Abl images to capture the integrated density (IntDen) of nuclear Abl. To capture the IntDen of cytoplasmic Abl, the masks were used to fill in the nuclei with black, and the AP tool was used again to generate masks of individual cells. The percentage of nuclear Abl intensity was calculated by dividing nuclear IntDen by the sum of nuclear plus cytoplasmic IntDen for each cell, and the median and interquartile range of values from at least 20 cells per sample are shown in the figures.

Immunoblotting

Cell pellets were lysed in RIPA buffer (25 mM Tris-HCl, pH 7.6, 10% glycerol, 1% NP40, 0.5% sodium deoxycholate, 1x protease inhibitors [Roche], 150 mM sodium chloride, 50 mM sodium fluoride, 10 mM sodium beta-glycerophosphate, 10 mM sodium orthovandate, 10 mM sodium pyrophosphate, 1 mM phenyl-methanesulfonyl-fluoride). Proteins were separated using SDS–PAGE and transferred onto nitrocellulose membranes (Millipore). Membranes were blocked for 1 h at room temperature, incubated with anti-Abl (8E9) (1/500) and anti-actin (1/2000) from Sigma Aldrich for 1 h, washed and incubated with secondary antibody (Anti-mouse: HRP-linked), and developed using ECL reagents (Pierce).

Retrovirus packaging and infection

Each of Abl^{WT}, $Abl^{\mu NLS}$, and Abl^{KD} stably expressed in *Abl-µNLS* MEFs by retroviral infection. BOSC23 cells were transfected with retroviral vector pMSCV expressing Abl^{WT}, $Abl^{\mu NLS}$, or Abl^{KD}. Culture media collected at 48 h after transfection were filtered and added to *Abl-µNLS* MEFs with polybrene (4 µg/ml). Infected cells were then selected for resistance to hygromycin (150 µg/ml).

Transfection

Genetran (Biomiga) was used to transfect HEK239T cells with miR-34c-minigene and pCDNA3-AblPPn plasmid DNA (Tu *et al*., 2015). Transfected cells and their media (for EV isolation) were collected 24 h after transfections. RNAiMAX was used to transfect MEFs with control mimic (CGGUACGAUCGCGGCGGGAUAUC) and miR-34c mimic (AGGCAGUGUAGUUAGCUGAUUGC) (Sigma). The transfection efficiency was ~80%, as determined by siGLO

green (Dharmacon). The ROS levels in live transfected cells were measured at 24 h posttransfection as described above.

RNA measurements

A SeraMir Exosome RNA amplification kit (System Biosciences) was used to extract RNA from EV pellets. Total cellular RNA was extracted using TRIzol (Life Technologies). Synthesis of cDNA was carried out using an ABI reverse transcription kit (Life Technologies). For measurements of mature miR-34c, stem-loop primer was used for reverse transcription (Tu *et al.*, 2015). U6 was used as the reference gene for normalization of miR-34c abundance. Real-time PCRs were carried out using a StepOnePlus system. Subtraction of the reference gene CT value from the experimental gene CT value generated the normalized ΔCT. Relative abundance was then calculated as $2^{-\Delta\Delta CT}$, where ΔΔCT values were ΔCT of vehicle-treated or vector transfected cells subtracted from ΔCT of sample. Primer sequences:

U6-F: CTCGCTTCGGCAGCACA, U6-R: AACGCTTCACGAATTTGCGT,

Stem-loop miR34c: GTCGTATCCAGTGCAGGGTCCGAGGTATTCGCACTGGATACGACGCAATC,

q-miR34c-F: AGGCAGTGTAGTTAGCTG, q-miR-R: GTGCAGGGTCCGAGGT

Statistical analysis

The statistical analyses were performed using Graph-Pad Prism 6. For clonogenic survival and quantitative reverse transcription-PCR measurements the mean ± SD from three independent experiments were analyzed using one-way analysis of variance (ANOVA). For PKH26 quantification, the mean ± SD of total mean gray values from at least six images per sample were analyzed by one-way ANOVA. For ROS measurements, the DCFDA/CTR ratios from 200–600 cells from one to three independent experiments per sample were ranked across samples and the mean ranks analyzed using the nonparametric Kruskal–Wallis test. For nuclear Abl quantification, the percent nuclear IntDen from 20–30 cells per sample were ranked across samples and the mean ranks analyzed using the nonparametric Kruskal–Wallis test. For each statistical test, ns: not significant, $*P \le 0.05$, $**P \le 0.01$, $***P \le 0.001$, $****P \le 0.0001$.

ACKNOWLEDGMENTS

We thank Chenhui Bian, Neal Shah, and Louis Nguyen for excellent technical assistance. We thank Andrea Ventura, Memorial Sloan Kettering Cancer Center, New York, for the miR34^{WT} and miR34^{TKO} primary MEFs. We thank Clarke Chen and Johnny Akers for helping with the nanoparticle tracking analysis.

REFERENCES

Akers JC, Ramakrishnan V, Nolan JP, Duggan E, Fu CC, Hochberg FH, Chen CC, Carter BS (2016). Comparative analysis of technologies for quantifying extracellular vesicles (EVs) in clinical cerebrospinal fluids (CSF). PloS One 11, e0149866.

Baskaran R, Wood LD, Whitaker LL, Canman CE, Morgan SE, Xu Y, Barlow C, Baltimore D, Wynshaw-Boris A, Kastan MB, Wang JY (1997). Ataxia telangiectasia mutant protein activates c-Abl tyrosine kinase in response to ionizing radiation. Nature 387, 516–519.

Burdak-Rothkamm S, Rothkamm K, Prise KM (2008). ATM acts downstream of ATR in the DNA damage response signaling of bystander cells. Cancer Res 68, 7059–7065.

Chang TC, Wentzel EA, Kent OA, Ramachandran K, Mullendore M, Lee KH, Feldmann G, Yamakuchi M, Ferlito M, Lowenstein CJ, *et al* (2007). Transactivation of miR-34a by p53 broadly influences gene expression and promotes apoptosis. Mol Cell 26, 745–752.

Chaudhry MA (2014). Radiation-induced microRNA: discovery, functional analysis, and cancer radiotherapy. J Cell Biochem 115, 436–449.

Cocucci E, Racchetti G, Meldolesi J (2009). Shedding microvesicles: artefacts no more. Trends Cell Biol 19, 43–51.

Concepcion CP, Han YC, Mu P, Bonetti C, Yao E, D'Andrea A, Vidigal JA, Maughan WP, Ogrodowski P, Ventura A (2012). Intact p53-dependent responses in miR-34-deficient mice. PLoS Genet 8, e1002797.

Gong JG, Costanzo A, Yang HQ, Melino G, Kaelin WG Jr, Levrero M, Wang JY (1999). The tyrosine kinase c-Abl regulates p73 in apoptotic response to cisplatin-induced DNA damage. Nature 399, 806–809.

He L, He X, Lim LP, de Stanchina E, Xuan Z, Liang Y, Xue W, Zender L, Magnus J, Ridzon D, *et al.* (2007). A microRNA component of the p53 tumour suppressor network. Nature 447, 1130–1134.

Jelonek K, Widlak P, Pietrowska M (2016). The influence of ionizing radiation on exosome composition, secretion and intercellular communication. Protein Pept Lett 23, 656–663.

Kaidi A, Jackson SP (2013). KAT5 tyrosine phosphorylation couples chromatin sensing to ATM signalling. Nature 498, 70–74.

Komarova EA, Diatchenko L, Rokhlin OW, Hill JE, Wang ZJ, Krivokrysenko VI, Feinstein E, Gudkov AV (1998). Stress-induced secretion of growth inhibitors: a novel tumor suppressor function of p53. Oncogene 17, 1089–1096.

Leach JK, Van Tuyle G, Lin PS, Schmidt-Ullrich R, Mikkelsen RB (2001). Ionizing radiation-induced, mitochondria-dependent generation of reactive oxygen/nitrogen. Cancer Res 61, 3894–3901.

Mao A, Liu Y, Zhang H, Di C, Sun C (2014). microRNA expression and biogenesis in cellular response to ionizing radiation. DNA Cell Biol 33, 667–679.

Mineo M, Garfield SH, Taverna S, Flugy A, De Leo G, Alessandro R, Kohn EC (2012). Exosomes released by K562 chronic myeloid leukemia cells promote angiogenesis in a Src-dependent fashion. Angiogenesis 15, 33–45.

Mladenov E, Li F, Zhang L, Klammer H, Iliakis G (2018). Intercellular communication of DNA damage and oxidative status underpin bystander effects. Int J Radiat Biol, doi: 10.1080/09553002.2018.1434323.

Mukherjee D, Coates PJ, Lorimore SA, Wright EG (2014). Responses to ionizing radiation mediated by inflammatory mechanisms. J Pathol 232, 289–299.

Preyer M, Shu CW, Wang JY (2007). Delayed activation of Bax by DNA damage in embryonic stem cells with knock-in mutations of the Abl nuclear localization signals. Cell Death Differ 14, 1139–1148.

Prise KM, O'Sullivan JM (2009). Radiation-induced bystander signalling in cancer therapy. Nat Rev Cancer 9, 351–360.

Raver-Shapira N, Marciano E, Meiri E, Spector Y, Rosenfeld N, Moskovits N, Bentwich Z, Oren M (2007). Transcriptional activation of miR-34a contributes to p53-mediated apoptosis. Mol Cell 26, 731–743.

Shaul Y, Ben-Yehoyada M (2005). Role of c-Abl in the DNA damage stress response. Cell Res 15, 33–35.

Shurtleff MJ, Temoche-Diaz MM, Karfilis KV, Ri S, Schekman R (2016). Y-box protein 1 is required to sort microRNAs into exosomes in cells and in a cell-free reaction. Elife 5, e19276.

Sridevi P, Nhiayi MK, Wang JY (2013). Genetic disruption of Abl nuclear import reduces renal apoptosis in a mouse model of cisplatin-induced nephrotoxicity. Cell Death Differ 20, 953–962.

Thery C, Amigorena S, Raposo G, Clayton A (2006). Isolation and characterization of exosomes from cell culture supernatants and biological fluids. Curr Protoc Cell Biol Chapter 3:Unit 3 22.

Tkach M, Thery C (2016). Communication by extracellular vesicles: where we are and where we need to go. Cell 164, 1226–1232.

Tu CC, Zhong Y, Nguyen L, Tsai A, Sridevi P, Tarn WY, Wang JY (2015). The kinase ABL phosphorylates the microprocessor subunit DGCR8 to stimulate primary microRNA processing in response to DNA damage. Sci Signal 8, ra64.

Valadi H, Ekstrom K, Bossios A, Sjostrand M, Lee JJ, Lotvall JO (2007). Exosome-mediated transfer of mRNAs and microRNAs is a novel mechanism of genetic exchange between cells. Nat Cell Biol 9, 654–659.

Verma N, Tiku AB (2017). Significance and nature of bystander responses induced by various agents. Mutat Res 773, 104–121.

Wang JY (2014). The capable ABL: what is its biological function? Mol Cell Biol 34, 1188–1197.